Characterization of SrTi03 target doped with Co ions, SrCo Ti1−03−δ, and their thin films prepared by pulsed laser ablation (PLA) in water for visible light response

doi: 10.1016/j.apsusc.2017.04.130

Characterization of SrTiO3 target doped with Co ions, $SrCo_xTi_{1-x}O_{3-\delta}$, and their thin films prepared by pulsed laser ablation (PLA) in water for visible light response

Fumihiko Ichihara[1], Yuma Murata, Hiroshi Ono, Katsumi Tanaka*

Graduate School of Informatics and Engineering, The University of Electro-Communications, 1-5-1 Chofugaoka, Chofu, 182-8585, Japan

Cheowkeong Choo

Center for International Programs and Exchange, The University of Electro-Communications, 1-5-1 Chofugaoka, Chofu, 182-8585, Japan

[1]Present address:

*Corresponding author

e-mail: katanaka@ee.uec.ac.jp

ABSTRACT

$SrTiO_3$ (STO) and Co-doped $SrTiO_3$ (Co-STO) sintered targets were synthesized at 1573 K, then underwent pulsed laser ablation (PLA) to prepare their thin films. The targets showed clear XRD peaks of the STO until the doped Co amount reached 30% denoted as Co(30)-STO. Doped Co ions were substituted with octahedrally coordinated Ti ions as the Co^{2+} state, which was proved by the Co 2p satellite peaks in the X-ray photoelectron spectroscopy (XPS) spectra. The STO and Co(30)-STO targets were treated to evaluate their charge compensation as follows; sputtered by an Ar ion gun, exposed to air, reduction with hydrogen at 1073 K, then exposed to air, and oxidized at 1073 K. Following exposure of the Ar-sputtered target to the air,

charge transfer reactions occurred among Co^{2+},Ti^{3+}, O^{2-} and Sr^{2+} species which were clarified by their XPS spectra. The origin of two kinds of O 1s spectra detected at 530 and 533 eV was studied by these five treatments and was assigned to the bulk and surface oxygen species, respectively. The PLA of the STO and Co-STO targets was carried out in water at 355 nm and with a constant laser fluence. The atomic ratios of the Ti/Sr and Co/Sr as well as that for the two kinds of O 1s spectra of the PLA thin films were studied. The effect of the doped Co ions in the crystal structure of the thin films was studied by the XRD peak shift of the $SrTiO_3$ (110) face. Diffuse reflectance spectra revealed a quantum-sized effect for the r.t. deposited STO thin film, and a d-d transition and charge transfer band for the Co-STO targets. Photo-degradation of methylene blue was carried out on the PLA thin films under very weak power (0.7 mW) visible light at 460 nm from which a quantum yield was obtained to evaluate the role of the doped Co ions in the STO.

INTRODUCTION

Strontium titanate ($SrTiO_3$: hereafter denoted as STO) has been widely studied as a significant n-type semiconductor because of its stability, electronic properties and band-gap energy control by heteroatom doping, and as a result has been found to be applicable to oxide electronics[1,2], water splitting into H_2 and O_2 under UV light[3-6], one of the photo-catalysts with a perovskite structure[7] and an anode material for fuel cells.[8-11] The indirect band gap of the STO (3.1-3.7 eV) is too high to expect a response to visible light if we consider the advantage of solar energy use from the viewpoint of environmental benign technology. So far, many applications have been performed to control the band gap for the visible light response. For the photo-degradation of the dye molecules, visible light sensitive materials, such as CeO_2, were added[12,13] or Ag nanoparticles were added to the STO by surface plasmon resonance.[14] While doping hetero atoms into the STO has been done using the analogy with technologies found in TiO_2 systems[15,16], a bandgap (E_g) decrease was detected both experimentally[17] and theoretically.[18] In addition, the photo-catalytic activities have been successfully observed by doping. H_2 formation from methanol was found under visible light irradiation by co-doping Sb/Cr with the STO.[19] Visible light mediated photocatalytic activities were found in the co-doping systems such as S/C[20], La/N[21], Ag/Pb[22] and Cr/Ta.[23] An interesting question has arisen as to whether the doped Cr ions are substituted at both the A and B sites[24] or with only the A site.[25] Recently, it was reported based on EXAFS experiments and theoretical calculations that according to their thermal stability, La and Cr ions were substituted at the A and B sites into the STO, respectively.[26]

Many cations have already been doped into the STO. The A site substitution has been tried by doping Ca^{2+}[27,28], Ba^{2+}[29], Pb^{2+}[30], Bi^{2+}[31] and Mn^{2+}[32] for phase transition and ferroelectric behavior, and Ba^{2+}[33] for tunable microwave applications. Considering the ionic radii of these cations, which can be substituted with Sr^{2+} (A site) coordinated with 12 lattice oxygen atoms, the relation between the antiferro distortive transition temperature and tolerance factor was

considered, and the Sr vacancies were suggested by doping La^{3+}, Gd^{3+} and Y^{3+} into the STO.[34] Because of the presence of other perovskite structure materials, such as $SrFeO_3$ and $SrCoO_3$, Fe and Co ions have been tried to be substituted at the B site (Ti^{4+}) in the STO. In the Fe ion doped STO, the bandgap values gradually decreased as a function of the Fe content.[35-37] Whereas the oxidation state of the Fe ion should be 4+ in $SrFeO_3$[38], oxygen vacancies have been assumed in these Fe doped STO systems. It was reported that oxygen vacancies formed in the Fe doped STO will act as an electron trap which retards recombination of the photo-excited e-h pairs.[35] At the same time, shake-up satellite peaks detected in the Fe 2p XPS spectra were explained due to Fe^{3+}, which was responsible for the oxygen vacancies. In the Co doped STO systems, it has been reported that Co ions are doped in the B sites of the STO structure.[39-42] It seems conclusive that Co ions are doped in the divalent state (Co^{2+}) at the Ti^{4+} sites with octahedral coordination since the Co^{4+} state can be restrictively present at an extremely high pressure (6 GPa) in $SrCoO_3$[43], and strong Co 2p XPS satellite peaks detected in Co-STO system can be assigned due to the high-spin Co^{2+} state (d7: 4 e in t_{2g} and 3 e in e_g).[44] It is reported that Co ions can be substituted at the B sites in $BaTiO_3$ with a perovskite structure, in which Co^{2+} ions with a paramagnetic (high spin) configuration coexist with the diamagnetic Co^{3+}, and after annealing, and the Co ions are stabilized as Co^{2+} species with mainly an octahedral and trigonal symmetry (about 5%).[45] Although no oxygen vacancies are expected for the stoichiometric $SrSi_xTi_{1-x}O_3$ system[46], oxygen vacancies with the same amount as the doped Co^{2+} should be formed in the STO. So far, the oxygen vacancy has been suggested to be responsible for the ferromagnetism (FM) in the Co-doped TiO_2[47], In_2O_3[48] and STO systems.[44,49-52] Based on density functional calculations, FM is sensitive to the arrangement of most adjacent Co ions and oxygen vacancies and the presence of an oxygen vacancy makes both E_g and the lattice parameter larger.[51] It was also suggested that the charge-compensating oxygen vacancies should be located outside the B site surrounding octahedral.[45] Therefore, the relaxation effect on the Co-STO bulk by the formation of oxygen vacancies is one of the most

significant subjects to study. In the present study, we specially focused on (i) how the STO bulk is charge compensated in the presence of Co ions after Ar sputtering, exposed to air and reduction with hydrogen at high temperature, (ii) the role of the Co content on the stability of the STO bulk and the surface. At the same time, we prepared thin films of STO and Co-doped STO by PLA in water for the visible light photo-degradation of organic dye molecules. The focused points are (iii) the effect of Co ions on the preparation of the PLA thin films, (iv) stability of the studied thin films by annealing at high temperature, (v) assignment of two kinds of O 1s species detected at different BE values, and (vi) visible light photo-degradation activity of the PLA thin films.

Pulsed laser ablation (PLA) has been used for the thin film preparation. For instance, STO[53,54] and other perovskite compound[55-57] thin films were prepared by PLA in an ultra-high vacuum system and/or at ambient gas pressure. It will be possible to prepare multi-component thin films by PLA methods using many target source materials. In addition, this method has the advantage which can make a large area thin film from a bulk material. Recently the PLA method has been extensively developed to prepare size-controlled ultrafine particles in an aqueous solution. For instance, titania nanoparticles applicable for the photo-catalytic reaction have been synthesized in water media.[58] Whereas PLA has been normally extended to prepare fine particles in solutions, however, the PLA of STO or Co-STO in water has not yet been applied. We prepared STO and Co-STO sintered targets and characterized them by XRD and XPS, and in addition, PLA in the solution was tried using these targets and obtained PLA thin films that were characterized and used for the photo-degradation of an organic dye under visible light irradiation.

EXPERIMENTAL

The STO target for the PLA in water was prepared as follows; initially pre-heating a mixture of a 1:1 molar ratio of $SrCO_3$ and TiO_2 at 1273 K for 12h. The obtained STO powder

was then pressed as a pellet with a 20-mm diameter, then post-heated at 1573 K for 24 h in air using our electronic oven (max temp: 1773 K). The Co-STO samples were prepared by adding the corresponding amount of Co_3O_4 to a mixture of $SrCO_3$ and TiO_2, in which the Co (Ti) amounts were 1 (99), 3 (97), 5 (95), 10 (90), 20 (80) and 30 (70) % of the Sr amount. The corresponding Co-STO targets were denoted as Co(1), Co(3), Co(5), Co(10), Co(20) and Co(30)-STO, respectively. The procedures for the heating and pressing to prepare the Co-STO targets were the same as those for the STO target.

The core level and valence band photoelectron spectra were recorded by X-ray photoelectron spectroscopy (XPS; VG-ESCA Mark II), in which Al Kα radiation (1486.6 eV) and a pass energy were employed at 100 W and 50 eV, respectively. The charge-up of the binding energy (BE) values was referenced to the C 1s peak at 285.6 eV as the internal standard. The BE values of Ti 2p3/2 and O 1s on the STO and Co-STO were 458.6 and 530.0 eV, respectively. These values are quite reasonable and almost the same values as reported for TiO_2.[58,59] The BE value of O 1s was reported to be 529.85 eV for $SrTiO_3$.[60] In $BaTiO_3$ with the same perovskite structure, the BE values of Ti $2p_{3/2}$ and O1s XPS spectra were reported to be 459.8 and 531.0 eV[61] and 459.0 and 530.3 eV, respectively.[62] The difference in the BE values between O 1s and Ti $2p_{3/2}$ was almost constant at 71.2-71.4 eV even under a different Fermi edge. In the present paper, the BE values of Ti $2p_{3/2}$ for Ti^{4+} in STO and Co-STO were referenced to be 458.6 eV. One of the O1s signals showed a peak at 530 eV. Ar sputtering was carried out using the same XPS system.

The pulsed laser ablation (PLA) in water was carried out to prepare STO and Co-STO thin films by the same method as previously reported for preparing titania nanoparticles except for the laser wavelength.[58] The third harmonics (355 nm, 10 Hz) of a Nd:YAG pulsed laser (Continuum,Surelite-10) were reflected with the mirror and vertically supplied to the STO and Co-STO pellets in distilled water through a quartz lens with a focal length of 150 mm. The energy density focused on the target, the so-called fluence, was estimated from the

supplied laser energy and the spot size, which were measured by a laser power meter (OPHIR, model AN/2) and a burn paper, respectively. In the present study, a constant fluence of 0.5 J/cm^2 and a constant water layer thickness (distance between the target surface and water-air interface) of 0.6 cm were used. The nanoparticle solvated water solution was dropped on the 10x10x1 mm^3 quartz substrate and dried in air at a temperature controlled below 323 K. The obtained thin films were denoted as "r.t. prepared PLA thin films" in the present study. The $SrCO_3$ peaks could be detected in the XRD experiments of the r.t. prepared PLA thin films so that they were annealed in air or reduced with H_2 at 873 to 1073 K, at which the $SrCO_3$ XRD peaks completely disappeared.

The photo-catalytic activity was studied by the photo-degradation of methylene blue under visible light irradiation. The PLA thin films were deposited on the quartz substrates and were placed in the bottom of plastic cells. A methylene blue (MB) water solution ($1x10^{-4}$ M) filled the cells and a blue photodiode light at 460 nm irradiated the PLA thin films through the MB solution at the power of 0.7 mW. The photo-degradation activity was measured using the Lambert-Beer law at 667 nm (MB absorption maximum) by a ultraviolet-visible (UV) spectrometer (Jasco V-660). Blank experiments were simultaneously carried out under the same conditions except for the PLA thin films.

RESULTS and DISCUSSION

1. Characterization of STO and Co doped STO targets

The crystal structure of the targets for the PLA in water, STO and Co(1) to Co(30)-STO were studied by X-ray diffraction. As shown in Fig. 1, sharp and intense peaks were detected at 2θ of about 32, 39, 46, 57 and 68 degree, which were assigned to the (110), (111), (200), (211) and (220) faces of the perovskite STO structure, respectively. These spectra indicated sufficient crystallinity to use then for the PLA experiments as the targets. The XRD peaks of the STO shifted to higher 2θ values by the Co doping, which implies that the inter-planar distance

diminishes by the Co doping. The ionic radii of Sr^{2+}, Ti^{4+} and Co^{2+} were reported to be 0.118, 0.068 and 0.074 nm, respectively.[63] The ionic radius of the Co ions depends not only on the oxidation state, but also whether in the high spin (HS) or low spin (LS) states. It was reported that ionic radius of the HS state of Co4+ was 0.053 nm whereas the Co^{3+} and Co^{2+} ions had radii of 0.061 and 0.075 nm for the HS states and 0.055 and 0.065 nm for the low spin (LS) states, respectively.[64] The lattice parameter decreased when the Sr vacancy was formed or the A site in the STO structure was substituted with another ion of a much smaller radius.[65] Similarly, for the B site substitution in the STO, Co^{4+} ions could replace with Ti4+ to decrease the lattice parameter of STO. However, it may be crucial to expect the Co^{4+} in STO since high oxygen pressure is required to prepare the stoichiometric perovskite $SrCoO_3$ containing Co^{4+}.[43] It is difficult to explain the substitution of Co^{2+} for Ti^{4+} in the STO by taking only the ionic radius into account. Lattice parameters were refined by the Rietvelt method to explain the statistical distribution of the Ti and Co species of the B site in the STO.[39] In addition, the cationic substitution did not significantly change the structure because lattice parameter monotonously diminished as a function of x in $SrTi_{1-x}Co_xO_{3-\delta}$ obeying Vegard's law which was expected for a solid solution.

STO and Co(30)-STO were treated in order to study the charge compensation among the constitutional ions. Co 2p, Ti 2p, O 1s, Sr 3d and their valence spectra are shown in Figs.2, 3, 4, 6 and 7, respectively. Notations in the figures show the XPS spectra of samples treated in the sequence as follows: a) heated in air at 1073K, b) Ar sputtered at 5 kV, 20 μA for 3 min., c) then exposed to air, d) reduced with H_2 at 1073K, and e) re-heated in air at 1073K. The samples following Ar sputtering were measured by XPS in situ without exposure to air. The other samples were exposed to air after each treatment, then transferred to the XPS chamber to be analyzed.

The Co 2p spectra of the Co(30)-STO target are shown in Fig. 2. On the target, which was oxidized in air at 1073 K, the binding energies (BEs) of the Co 2p peaks were detected at 780.0

and 795.9 eV which were accompanied by broad signals that peaked at 786.0 and 804.6 eV (spectrum a). The first two peaks correspond to Co $2p_{3/2}$ and $_{1/2}$, while the broad signals are assigned to satellite peaks. After the Ar sputtering, the Co 2p peaks shifted to the lower BE side and detected at 777.7 and 792.6 eV, however, the satellite peaks almost disappeared (spectrum b). When the sputtered sample was exposed to air, two Co $2p_{3/2}$ peaks were detected at 777.8 and 780.7 eV (spectrum c). Compared to the spectrum after the Ar sputtering, the former decreased and the latter increased the peak intensity which accompanied the nearby satellite appearance at around 785 eV. Next, the Ar sputtered Co-STO sample was reduced with H_2 at 1073K, then exposed to air at r.t. The Co 2p XPS spectrum showed two kinds of $2p_{3/2}$ signals at 777.8 and 780.7 eV (spectrum d). The intensity of the latter species was dominant. The XPS spectrum for the sample re-oxidized at 1073 K (spectrum e) was very similar to that recorded for the oxidized sample (spectrum a). A broad signal at around 770 eV corresponds to the Co LMM Auger transition by the Al Kα radiation.

The BE values of Co $2p_{3/2}$ for the Co^{2+} (780 eV) and Co^{3+} ions (780.2 eV) in the perovskite structure are very close.[66] The spin-orbit sprit that is the BE difference between the $2p_{3/2}$ and $_{1/2}$ is one of the significant results to distinguish Co^{2+} and Co^{3+}. The value is 15.5-16 eV for the high spin Co^{2+}, while 15 eV for the low-spin Co^{3+}.[67-71] In our experiments, the value of about 16 eV was observed. Whereas only small satellite peaks can be detected in the low-spin Co^{3+}[72], strong satellite peaks have been detected in the high-spin Co^{2+} (d^7).[73,74] While the origin of the Co^{2+} satellites is explained by the change in the d-d coupling due to a strong electron-electron interaction caused by the high spin state, that is, the interaction between the O 2p electrons and Co valence electrons causes charge transfer from O 2p to Co 3d which produces many possibilities for the final states with respect to the photoelectron ejection.[75] It has been reported that the tetrahedrally coordinated Co^{2+} shows peaks at 780.5 eV for the $2p_{5/2}$ without satellites.[76,77] Base on these results, we conclude that Co ions in the STO are octahedrally coordinated in the high spin Co^{2+} state, which the Ti^{4+} sites in the STO are replaced.

The Co $2p_{3/2}$ was detected at 777.7 eV after Ar sputtering. The Co $2p_{3/2}$ of the metallic Co is reported to be 778.2 eV[78] Therefore, the species at 777.7 eV will be assigned to the Co^{0+} state. The Co^{0+} species were partially observed on the sample reduced with H_2 at 1073 K as well as on the air-exposed Ar sputtered sample. The species could only selectively be produced by severe reduction after Ar sputtering. The metallic Co species could be changed to octahedral Co^{2+} species in the STO after exposing the sputtered sample to air. The reversibility between Co^{0+} and Co^{2+} in the octahedral sites of STO is one of the striking results in the present study. Charge compensation in the STO and Co-STO after Ar sputtering is also one of the more interesting results.

The Ti 2p spectra of STO and Co(30)-STO are shown in Fig. 3. The Ti $2p_{3/2}$ and $_{1/2}$ peaks were detected at 458.6 and 464.3 eV, respectively, which were assigned to Ti^{4+}. The broad Ti $2p_{3/2}$ and $_{1/2}$ signals due to Ti^{3+} were observed on the lower BE side of the Ti^{4+} signals both in the STO and Co(30)-STO samples after Ar sputtering (spectrum b of both STO and Co-STO in Fig.3). A trace amount of Ti^{3+} species remained after exposing the Ar sputtered STO sample to air (spectrum c of STO). They will remain in the STO bulk. Considering that the spin-orbit sprit value is 5.7 eV between the Ti $2p_{3/2}$ and $_{1/2}$ and the BE value of Ti $2p_{3/2}$ for Ti^{3+} is 2.5 eV lower than Ti^{4+}[59], the Ti 2p spectra after Ar sputtering were deconvoluted to Ti^{4+} and Ti^{3+}. The concentration of Ti^{3+} was 26.0 and 20.5 % for STO and Co-STO, respectively. It was noted that Co^{2+} replaced from the octahedral Ti^{4+} species was almost completely reduced to metallic Co after the Ar sputtering in Co-STO as shown in Fig. 2. In other words, the amount of Ti^{3+} in the Co-STO seems to be compensated for by the metallic Co. The electrons to reduce the octahedral Co^{2+} species are produced by the reaction from Ti^{3+} to Ti^{4+}.[79] Trivalent Ti ions can reduce Fe^{3+} to Fe^{2+} in solution.[80] Therefore, the overall reaction can be descried as follows.

$$2\ Ti^{3+} + Co2+ \rightarrow 2\ Ti^{4+} + Co^{0+} \qquad (1)$$

As a result, the reduction of Co^{2+} could proceed by the formation of Ti^{3+} during Ar sputtering.

The O 1s spectra of STO and Co(30)-STO are shown in Fig. 4. These O1s spectra could be analyzed by the two species with the full width at half maximum (fwhm) values of 2.6-2.8 eV and 2.3-2.5 eV, respectively. The two species were deconvoluted into two peaks at 530 and 532.5-533.0 eV. Hereafter, they are denoted as O(I) and (II), respectively. The change in the relative intensity of the O(II) to O(I) species following the a-e sequence in Fig. 4 is plotted in Fig. 5. The intensity ratio of the two species, hereafter denoted as II/I, was higher than 1.0 in the STO and decreased to about 0.6 in the Co-STO. The II/I ratio decreased after the Ar sputtering both in the STO and Co-STO. It is significant to note that the peak position of O(I) shifted to the higher BE side with about 1 to 2 eV but that of O(II) showed no shift after the Ar sputtering for both the STO and Co-STO, as shown in Fig. 4-c. Regarding the air exposed samples, whereas the II/I ratio was almost the same as that of the Ar sputtered sample for the STO, the II/I ratio increased from 0.31 to 0.44 for the Co-STO. The O(II) peak position did not change at all in all the experiments as well as the following Ar sputtered sample that was exposed to air.

The Sr 3d spectra of STO and Co(30)-STO are shown in Fig. 6. The Sr $3d_{5/2}$ and $_{3/2}$ peaks were not well analyzed because the fwhm of the peaks was comparable to the spin-orbit sprit value (2 eV). The Ar sputtered STO and Co-STO samples did not show a BE shift as shown in Fig.6-c. However, the Sr 3d spectra shifted to the lower BE side about 0.3 eV when the Ar sputtered samples were exposed to air. The BE value of Sr $3d_{5/2}$ was observed at 134 eV for the STO and Co-STO in Fig. 6. The BE value of Sr $3d_{5/2}$ for the metallic Sr is reported to be 133 eV.[81] Therefore, the 0.3 eV shift to the lower BE side implies that the oxidation state of the Sr ions is $1+\delta$ ($0<\delta<1$). The STO and Co-STO showed different Sr 3d spectra after the H_2 reduction at 1073 K followed by exposing them to air at r.t. The metallic Co was detected on Co-STO (Fig. 2-d). This implies a charge compensation or a redox mechanism between the Sr, Ti and Co ions in the surface region, which will be discussed later.

The valence band spectra of STO and Co(30)-STO are shown in Fig. 7. Two peaks were observed at 5-8 and 20 eV in all the spectra. One can see the shoulder at 21-22 eV on the STO in Fig. 7-a so that at least one more species is present that overlaps with the intense peak at 20 eV. The peaks at 20 and 23 eV were assigned to the O 2p and the overlapping of Sr and O 2s, respectively.[82] At the same time, the O 2p at 5-8 eV was deconvoluted into two species at 4.9 and 7.3 eV which were assigned as the O 2π and σ bonding orbitals, respectively. Two states were also detected in $BaTiO_3$ which were attributed to the pure oxygen states and O 2p-Ti 3d mixed states.[62] One another valence band species was detected at 7.8 eV, which was mainly assigned to the pdσ interaction in $BaTiO_3$.[61] The peak at 26 eV was very intense in the STO treated with O_2 at 1073 K (Fig. 7-a) and re-oxidized with O_2 (Fig. 7-e) at the same temperature. In Fig. 4, the O(II) species was most intensively detected in both samples. Therefore, the peak at 26 eV will be associated with the O(II) species. A signal was detected near the Fermi edge in the Ar sputtered Co-STO sample as shown by the arrow in Fig. 7-b. It was assigned due to the metallic Co. The peak was attenuated in the air exposed Co-STO sample, but was still present as a weak signal near the Fermi edge in Fig. 7-c. The same peak was detected in Co-STO reduced with H_2 at 1073 K in Fig. 7-d. It should be noted that the H_2 reduced sample was then exposed to air and transferred to the XPS chamber.

The obtained experimental results are summarized in Figs. 3-6. In the STO and Co-STO after Ar sputtering, a) Ti^{4+} species were reduced to Ti^{3+}, b) the intensity of the O(II) species decreased, c) the O(I) peak position shifted to the higher BE side, and d) the Sr 3d peak position showed no BE shift. In addition, the Co^{2+} species were reduced to metallic Co in the Co-STO. When the Ar sputtered samples were exposed to air, e) the Ti^{3+} species were oxidized to Ti^{4+}, f) the O(I) peak position showed no BE shift, and g) the Sr 3d peak shifted to the lower BE side for both the STO and Co-STO. The difference between the air-exposed STO and Co-STO was observed for the II/I ratio, that is, the ratio increased on Co-STO although the

ratio showed no change on STO. After the Ar sputtering, the following reaction will occur, where αδ corresponds to unity.

$$Ti^{4+} + \alpha O^{2-} \rightarrow Ti^{3+} + (\alpha - x)O^{(2-\delta)-} + (x/2)O_2 \quad (2)$$

The O(II) species decreases about half after the Ar sputtering so that the remaining O(I) species are charged δ+ as a result of the charge compensation. Simultaneously, the reduction reactions of Ti^{4+} to Ti^{3+}, and Co^{2+} to Co cause a decrease in the O(II) species, whereas the charge distribution of Sr 3d is not affected. The behavior of O(II) seems to be related to the oxygen atoms surrounding the octahedral Ti^{4+} sites, which can be substituted by the Co^{2+} species.

The shift of the Sr 3d spectra to the lower BE side observed in the air exposed samples in Fig. 6 will imply the electron transfer from the Ti^{3+} to Sr^{2+} ions. The BE shift of the O(I) species was simultaneously detected with the electron transfer. Accordingly, the O(I) and O(II) species will be assigned to the bulk and surface oxygen, respectively. Because electrons should be supplied from the bulk of the Ar sputtered samples after exposing them to air where oxygen vacancies are recovered as lattice oxygens, the following reaction will explain the electron transfer by the formation of O^{2-} species. In the assumed reaction, monovalent a Sr ion is required whereas the observed valence state will be 1+δ.

$$3\ Ti^{3+} + [\quad] + Sr^{2+} + (1/2)O_2 \rightarrow 3\ Ti^{4+} + [O]^{2-} + Sr^{+} \quad (3)$$

The O1s spectra of Co containing oxides were observed as a single peak at 530 eV for CoO(100) and a main peak at 530 eV with a shoulder at around 531.5 eV for the Co_3O_4 single crystal cracked in ultra-high vacuum (UHV) chamber, while some peaks appeared at 529.6, 531.2 and 533 eV for $NiCo_2O_4$.[83] Three O 1s peaks of $NiCo_2O_4$ were assigned to the lattice, intrinsic surface species and OH groups. Similarly, three O 1s species were detected at 529.9, 531.7 and 532.5 eV for the $SrTiO_3$ nanoparticles, which were assigned to the lattice oxygen, oxygen ions in the oxygen vacancies and adsorbed H_2O, respectively.[42] Two peaks were apparently observed for the O1s species in $La_{1-x}Ca_xCoO_3$, which were analyzed with four

species at 528.6, 530.6, 531.6 and 533.1 eV for the lattice oxygen, adsorbed O_2^{2-}/O^- species, OH^- and molecular water, respectively.[84] While, the O 1s spectra were analyzed for species with BE values at 528.6, 529.8 and 532.5 eV in $La_xSr_{1-x}CoO_{3-\delta}$.[85] The lowest BE species could be assigned to the lattice, while the intermediate species was detected after deconvolution and the highest BE species was assumed to be surface oxides. It has been suggested that such species are associated with the surface termination layer of the perovskite structure layer (Sr-O) and surface oxygen species such as secondary phases and/or adsorbates, respectively.[81] Simultaneously, two Sr 3d species due to the lattice and surface were detected in $La_xSr_{1-x}CoO_{3-\delta}$.[85] Two O1s signals were observed at 528.5 and about 531-532 eV for the lattice oxygen and surface phases such as hydroxides and carbonates with the BE separation of about 3 eV in $La_xSr_{1-x}CoO_{3-\delta}$.[86] BE values for the Sr 3d and O 1s in $La_xSr_{1-x}CoO_3$ were 1.5 eV lower than those in $SrTiO_3$ at 131.6 and 530.7 eV.[81] According to these references, the O 1s species detected on the higher BE side at around 533 eV have been assumed to be surface OH groups.

The structure of STO is shown in Fig. 8. It is difficult to distinguish oxygen atoms surrounding the Ti^{4+}/Co^{2+} sites and Sr^{2+} sites because they are equivalent. To evaluate the origin of the O(II) species at 533 eV, two important results must be taken into account. a) The O(II) species diminished the intensity after substituting Co^{2+} ions for Ti^{4+} species, and b) the II/I intensity decreased after Ar sputtering for both the STO and Co-STO. In our experiments, the STO and Co-STO targets were sintered in the air at 1473 K so that the surface area of our targets should be too low to form OH groups of a comparable amount with bulk oxygen by exposing the targets to ambient water. Therefore, it is crucial to assign the O(II) species at 533 eV to the OH groups. The third significant result was that a charge density decrease of O(I) species which was represented as the higher BE side shift was only detected after Ar sputtering (Fig. 4-b). The formation of O vacancies and Ti3+ species should be significant as additional information for above mentioned cases a) and b), respectively. It is noted that the formation of O vacancies is not necessarily simultaneously accompanied by that of Ti^{3+} in the

Co-STO samples. There are two kinds of truncated surface structures for $SrTiO_3$, that is, the Sr ion terminated surface and Ti/Co terminated surface. They are denoted as the Sr-O and Ti-O surface for convenience. Assuming the STO surface to be exposed with the x-y plane in Fig. 8, the O(1) and O(2) ions are the surface oxygen in Sr-O and Ti-O surface, respectively. The substituting Co^{2+} for Ti^{4+} can be explained by one oxygen atom removal per one TiO_6 unit in the STO as follows.

$$Ti^{4+}O_6 \rightarrow Co^{2+}O_5 + (1/2)O_2 \qquad (4)$$

However, the oxygen vacancy is not necessarily formed in the $Co(II)O_6$ octahedra because the Co ion should be reduced. It is reported that Co^{2+} should work as an isolated defect in the bulk and charge compensating oxygen vacancies will be formed outside of the $(Ti/Co)O_6$ octahedra in $BaTiO_3$.[45] If our Co-STO system is in such a situation, the reversible redox reaction between the Co metal and Co^{2+}, which was detected in Fig. 2 after Ar sputtering and air exposure, will be possible and also reasonable. After Ar sputtering, the Ti^{3+} species will be formed by the following reaction.

$$Ti^{4+}—[O^{2-}]—Ti^{4+} \rightarrow Ti^{3+}—[\ ]—Ti^{3+} + (1/2)O_2 \qquad (5)$$

If the Sr-O plane composed of Sr(1) and O(1) is the outermost surface, O(1) should not be a candidate for reaction (5) since no connected Ti site to form Ti^{3+} exists. O(2) and O(3) are then the candidates. When the Ti-O plane composed of Ti ions and O(2) sites constitutes the outermost surface, not only O(2), but also O(3) in the bulk side will be a candidate for an oxygen vacancy for reaction (5). As a result, it is crucial to elucidate whether the outermost truncated surface is the Sr-O or Ti-O surface because of the high crystal symmetry of the cubic structure. Following Ar sputtering, the perovskite structure will probably be so damaged in the surface region that the valence states of the Sr and O ions should be compensated to maintain charge neutrality in the bulk since the conductivity in the surface region should be very high. Therefore, it is reasonable to explain the higher BE side shift of O(I) by reaction (2). It also infers that the surface oxygen O(II) decreased by the Ar sputtering and the bulk oxygen

O(I) should play a significant role in the charge compensation for reduction. The former and the latter explain the II/I ratio decrease and the higher BE side shift of the O(I) species. The surface region should have a higher conductivity than the bulk so that the surface O(II) species is not involved in the charge compensation as detected in the bulk O(I) species.

2. Characterization and photo-degradation activity of thin films prepared with PLA in water

The atomic ratios of Ti and Co to Sr in both r.t and 873 K prepared PLA thin films were studied by XPS. Not only these values, but also those measured in the targets for the PLA are shown in Fig. 9. The horizontal scale indicates the Co percentage n in the Co(n)-STO targets. The Co percentage n corresponds to ten times as much of mole fraction x in chemical formula $SrCoxTi_{1-x}O_{3-\delta}$. The Co/Sr ratios in the Co(n)-STO targets were almost the same as one tenth the Co percentage n, and as a result, showed a linear relation to n. The Co/Sr ratios detected in both the r.t. and 873 K prepared PLA thin films were also the same as those in the Co-STO targets. This result implies that the Co/Sr atomic ratio of the species formed during the PLA process will be the same as those in the corresponding Co-STO target. The Ti/Sr ratio in the STO target was 1.0 and the value in the Co-STO targets gradually decreased as the Co percentage n increased. The Ti/Sr ratio was 0.7 and the Co/Sr ratio was 0.3 in the Co(30)-STO target, whereas the former and the latter values were 0.8 and 0.2 in the Co(20)-STO target, respectively. These results clearly imply that the amount of Sr ions is equal to the summed amount of the Ti and Co ions in the Co-STO targets. This fact clearly indicates that Co ions can be substituted for the Ti ion sites, which proves that it is correct to represent our Co-STO target as $SrCoxTi_{1-x}O_{3-\delta}$. However, the Ti/Sr ratio was 2.57 for the r.t. prepared STO thin film, which increased to 2.11 after annealing at 873 K. The values of the Ti/Sr ratio in both the r.t. and 873 K prepared Co-STO thin films were also much higher than the stoichiometric value (1.0) in the STO and the value monotonously decreased as the Co percentage n in the Co(n)-STO target increased.

As mentioned in the PLA target section, two O 1s species were detected at 530 and 532.5-533.0 eV, not only in the STO target, but also in the Co(30)-STO target. These two species denoted as O(I) and O(II) species could be assigned to the bulk oxygen and surface oxygen, respectively. These two species were also observed in the PLA thin films. The values of the II/I ratio in the targets as well as the thin films are shown in Fig. 10. The value was 1.09 in the STO target and decreased to 0.35 in the Co(1.0)-STO target. The ratio gradually increased from 0.36 in the Co(10)-STO to 0.53 in Co(30)-STO target. While the ratio was 0.73 in the r.t. prepared STO thin film, the value decreased to 0.4 after annealing at 873 K. In the r.t. prepared Co-STO thin films, the values were 0.58, 0.23, 0.29, 0.45 and 0.5 in the thin films with n=3, 5, 10, 20 and 30 of Co(n)-STO, respectively, whereas the value was 1.36 at n=1. These II/I values decreased when the r.t. prepared PLA films were annealed at 873 K. These results are summarized as follows. (i) The II/I ratio in the STO decreased when the Co ions were doped. (ii) The minimum value was detected at a doped Co amount below 5 %. (iii) The ratio gradually increased at the Co content above 10%. (iv) The II/I ratio in the r.t. prepared PLA thin films decreased after annealing at 873 K. It is noted that (i), (ii) and (iii) hold true not only for the targets, but also for the PLA thin films. These four summarized results are studied based on the assignment of the O(I) and O(II) for the bulk and surface oxygen, respectively. It is deduced from (i) that the surface region is stabilized by the doped Co ions. It is suggested from (iii) that a new crystal phase, such as $SrCoO_3$, may appear to segregate, which will make the surface become less stable. In fact, very weak but sharp XRD peaks could be detected at 2θ degrees of 44 and 65 in the Co-STO targets with the Co content n greater than 10% in Fig. 1. In this sense, the most stable surface could be obtained in the Co(1)-STO and Co(3)-STO targets as an optimum condition, which is responsible for result (ii). The stability enhancement of the surface region by the presence of a small amount of Co ions and the suppression of the crystal stability caused by an extra amount of Co ions are responsible for the presence of the optimum Co amount in the Co-STO structure. Result (iv) is very significant in order to support the

validity of our assignment for O(I) and O(II), because the surface of the r.t. prepared PLD films should be stabilized and can be partially converted to that like the bulk after annealing at 873 K. The minimum value of the II/I ratio in the Co-STO thin films was much lower than that in the corresponding Co-STO targets, which will be discussed later.

The narrow region XRD spectra for the perovskite STO (110) face of the PLA thin films are shown in Fig. 11. Although the r.t. prepared STO thin film showed no typical signal, the STO (110) phase was clearly detected in the Co-STO thin films. When the r.t. prepared STO thin film was annealed in air at 873 K, the (110) peak clearly appeared at 32.15 degrees. These two results are significant regarding the role of Co in the PLD targets for the thin film preparation. The (110) peak position of the Co-STO thin films was elucidated. The (110) phase was detected at 32.3 to 32.32 degrees for the Co-STO thin films prepared from the PLA of the Co(1)-, Co(3) and Co(30)-STO targets, while the peak was detected below 32.3 degrees on those from the Co(5), Co(10) and Co(20)-STO targets. When these thin films were annealed at 873 K in air, the (110) peak was detected at 32.2 degrees in the Co-STO thin film prepared with the Co(1)-STO target and the peak position gradually shifted to higher 2θ values in the Co-STO thin films as the doped Co amount in the target increased. It is significant to note that whereas the $SrCO_3$ phase was clearly detected in the wide region XRD spectra of the r.t. prepared thin films, the corresponding XRD peaks disappeared after annealing at 873 K in air (data not shown).

The effects of theCo ions in the targets on the crystal structure of the prepared thin films are discussed. The first result to note is that the (110) XRD peak appeared when the r.t. prepared STO thin film was annealed at 873 K. The result implies that the precursor species for the STO structure formation or the very small-sized clusters, whose size are too small to be detected by XRD, are clearly formed. In other words, the presence of Co ions in the PLA targets will enhance the probability of the STO cluster formation increase and/or the size of the STO cluster under the PLA in water. This is one of the most significant effects of Co on the PLA in

water. The second result to note is that the (110) peak shift to the higher degree side was not monotonous in the r.t. prepared Co-STO thin films. The r.t. Co-STO thin films prepared from the Co(1) and Co(3)-STO targets showed a sharp (110) peak at 32.30 to 32.35 degrees that was the highest of all, which corresponded to that observed in the 873 K prepared thin film using the Co(30)-STO target. This result implies that the stable structure with the chemical formula, such as $SrCo_{0.3}Ti_{0.7}O_{3-\delta}$, can be formed in part and reveals the intense XRD peak. As the average Co/Sr ratio was quite low (~0.06), however, the Ti/Sr ratios were 2.2 to 2.4 for the r.t. Co-STO thin films prepared from the Co(1) and Co(3)-STO targets as shown in Fig. 9, and the $SrCo_{0.3}Ti_{0.7}O_{3-\delta}$ species and chemical formula, such as $SrTi_{1.1\text{-}1.2}O_x$, should be present at about 1: 0.7. Such a $SrTi_{1.1\text{-}1.2}O_x$ species can be assumed to be STO and will be homogeneously present. If we could assume that the $SrCo_{0.3}Ti_{0.7}O_{3-\delta}$ core is covered with amorphous STO, the surface should be unstable, and as a result, could make the II/I ratio of the O1s spectra the highest (~1.35) in the r.t. Co-STO thin films prepared from the Co(1)-STO target. It is noted that the II/I ratio was minimum (0.2-0.3) in r.t. thin films prepared from the Co(5) and Co(10)-STO targets, in which the XRD peak positions (32.25-32.30) were the same even after annealing at 873 K. These results infer that the surface is stabilized as the Co amount in the target increased and the homogeneous intermediate $SrCo_xTi_{1-x}O_{3-\delta}$ will be formed by the aid of the Co ions. The STO(110) face shifted to the lower 2θ degree side following annealing at 873 K.

Assuming that our samples obey the indirect transition, the Tauc plots of the r.t. prepared and 873 K prepared STO thin films, Co(20)-STO target, and the 873 K prepared thin film are shown in Fig. 12. The optical band-gap (E_g) of the r.t. prepared STO film was 3.6 eV. However, it shifted to 3.4 eV after annealing at 873 K. These results clearly imply that the quantum confinement effect could be detected in the r.t. prepared STO thin film. It is significant to note that no clear XRD peak was detected in the STO thin film in Fig. 11. Therefore, it is reasonable to conclude that the presence of the STO cluster with a size smaller

than the limit of the XRD detection is responsible for these results. In addition to a band at 3.4 eV, a broad and intense absorption was observed at around 2-3 eV for the Co(20)-STO target. Such an absorption was not clearly detected on the 873 K prepared PLD film using the Co(20)-STO target, but absorption continued in this region.

Regarding the absorption bands at 2-3 eV and 3.4 eV for the Co(20)-STO target, two possibilities will be considered as originating from the transition metal ions; one is the d-d transition due to the ligand field transition and the other is the charge transfer transition from the ligand to transition metal ions. The former could be detected in the lower energy regions than the latter for the Co(II) ions. In the Co^{2+} ortho-diphenolate complexes, absorption bands at 0.8, 1.5, 1.9 and 2.2 eV were assigned as ligand field transitions, and that at 3.3 eV was assigned as a charge-transfer transition from the ligand O pπ to Co^{2+}.[87] The transition energy for the d-d transition depends on the coordination number of the centered transition metal ions. For instance, the d-d transition was detected at 2.0 and 2.5 eV for the five-coordinate, while at 0.8 and 1.9 eV for the four coordinate Co^{2+} azo complexes.[88] It seems significant to compare the d-d transition energy of the tetrahedral to that of the octahedral coordination. The high spin state of Co^{2+} in thepseudo tetrahedral complexes shows 1.1-1.2 and 2.1-2.3 eV for d-d transition.[89] The d-d transition can be detected for Co^{2+} at 0.9-1.0, 1.6-1.7 and 2.1-2.3 eV in the tetrahedral complexes[90] and at 0.8-0.9 and 1.8-1.9 eV in the trigonal-planar mononuclear complexes.[91] Ab initio calculations explained the spin allowed ligand field transition energy in the octahedral transition-metal oxide clusters, and reported the calculated values of 0.81, 1.81, 2.69 and 2.57 eV for the experimentally detected values at 1.02, 1.98, 2.41 and 2.67 eV in the octahedral $[Co(H_2O)_6]^{2+}$.[92] As a result, it seems difficult to distinguish the coordination state of the centered Co^{2+} ions as to whether tetrahedral or octahedral from the viewpoint of the transition energy. However, it will be reasonable to assign the oxidation state of the Co ion to be divalent since their calculations reported the d-d transition energy at 1.45 and 2.65 eV instead of the experimental values at 2.06 and 3.09 eV for the octahedral $[Co(H_2O)_6]^{3+}$.[92]

Therefore, it will be reasonable to assign the absorption band at 2-3 eV in the Co(20)-STO target as the d-d transition due to octahedral Co^{2+} ions and that at 3.4 eV as the charge-transfer band due to the Opπ to Co^{2+} transition.

Finally, the photo-catalytic activities of the PLA thin films were studied under very weak visible light irradiation using a blue LED (460 nm, 0.7 mW). The samples were STO, Co(3)-, Co(10)- and Co(30)-STO, which were reduced with hydrogen at 873 K and transferred to the reaction vessel in air. The reason why we chose the 873 K reduced PLA thin films is shown in Fig. 13. The XRD intensities of the H_2 reduced PLD thin films were most intense of all the treatments, oxidized in O_2 at 873 and 973 K, and reduced with H_2 at 873, 973 and 1073 K. As shown in Table 1, the decomposed methylene blue (MB) was on the order of 10^{-2} μmol for each 5 h intervals since our visible light source power was very low (0.7 mW), but the reaction catalytically continued. More than one order less MB was decomposed at 460 nm as the blank experiments. Based on the results in Table 1, it is noted that the photo-catalytic activity of the STO thin film was enhanced on the Co-doped STO thin films by more than twice, and the activity increased as the Co content was increased. The photo-catalytic activity corresponded to the order of 0.65-5.76 x 10^{-4} as the quantum yield (photo-decomposed MB molecules per one photon of 460 nm) as shown in Table 2. It is noted that the quantum yield number is comparable to that for powdered visible-light sensitive photo-catalysts such as $MgIn_2O_4$ and reduced $CaWO_4$.[93,94] The crystal growth should increase the mobility of photo-generated electrons and holes, and as a result, enhance the photo-catalytic activity. The appearance of catalytic activity under visible light irradiation on the 873 K reduced STO thin film will be induced by the formed oxygen defects sites, of which the energy states could be formed in the position about 0.5-1.0 eV below bottom of the conduction band. These oxygen defect sites will be responsible for the visible light response, as suggested in above mentioned photo-catalysts.[93,94] The enhancement of photo-degradation activities on the 873 K reduced Co-STO thin films will originate from the aid of the Co ions.

Table 1.

Photo-catalytic activities for MB degradation under visible light irradiation at 460 nm with 0.7 mW on PLA thin films prepared using STO, Co(3)-, Co(10)- and Co(30)-STO targets which were reduced with hydrogen before use. The total photo-decomposed MB molecules for every 5 h reaction time are presented in the 10^{-2} μmol range.

Sample	0 – 5 h	5 – 10 h	10 – 15h
STO	1.97	3.25	2.15
Co(3)-STO	3.53	3.32	3.50
Co(10)-STO	4.93	5.26	5.80
Co(30)-STO	5.14	5.18	5.97

Table 2.

Quantum yield for MB photo-degradation activity under visible light at 460 nm with 0.7 mW on PLA thin films prepared using STO, Co(3)-, Co(10)- and Co(30)-STO targets which were reduced with hydrogen before use.

Quantum yield x 10^4						
STO	Co(1)	Co(3)	Co(5)	Co(10)	Co(20)	Co(30)
0.65	1.67	2.97	3.25	5.30	4.64	5.76

CONCLUSIONS

1. The amount of Sr ions is equal to the summed amount of Ti and Co ions in the Co-STO targets and doped Co ions are substituted for the octahedral Ti^{4+} sites as the divalent state in the STO, which proves that it is correct to represent our Co-STO target as $SrCo_xTi_{1-x}O_{3-\delta}$.

Oxygen vacancies simultaneously formed by Co-doping will not necessarily be formed in the $Co(II)O_6$ octahedra.

2. Ar sputtering causes severe reduction of Co-STO to form zero-valent Co and Ti^{3+} species. The percentage of Ti^{3+} formed in the Co-STO is lower than in the STO, which will be explained by the following reaction.

$$2\ Ti^{3+} + Co^{2+} \rightarrow 2\ Ti^{4+} + Co^{0+}$$

At the same time, further oxygen vacancies should be formed. After exposing the Ar sputtered STO and Co-STO targets to air, a kind of redox reaction proceeds between the Ti^{3+} and Sr^{2+} by covering the oxygen vacancies as followed.

$$3\ Ti^{3+} + [\quad] + Sr^{2+} + (1/2)O_2 \rightarrow 3\ Ti^{4+} + [O]^{2-} + Sr^{+}$$

3. Two kinds of oxygen species, O(I) and O(II), detected with the BE values at 530 and 533 eV will be assignable to the bulk and surface oxygen, respectively. The surface oxygen species O(II) diminishes by Co-doping and probably are stabilized as in the STO bulk.
4. The conductivity will be high enough in the surface for the surface oxygen to show no shift after Ar sputtering. However, the bulk oxygen shows an O 1s value shift to the higher BE side based on the following reaction, which will contribute to charge compensation by the formation of Ti^{3+}.

$$Ti^{4+} + \alpha O^{2-} \rightarrow Ti^{3+} + (\alpha - x)O^{(2-\delta)-} + (x/2)O_2$$

5. The r.t STO thin film with no XRD peaks shows a quantum size effect with a 0.2 eV band-gap shift. The r.t. thin films prepared by PLA using Co present targets show an STO crystal phase.
6. The Co/Sr atomic ratio of the species formed during the PLA process is the same as that in the corresponding Co-STO target, while the Ti/Sr ratios in both the r.t. and 873 K prepared Co-STO thin films are much higher than the stoichiometric value (1.0) in the STO.
7. The stability of the surface region for the Co containing r.t. prepared thin films, which can be evaluated by the II/I ratio of the two O 1s species, is less than that in the STO thin film

for the 1-3 %Co content, in which a mixture state of crystalline $SrCo_{0.3}Ti_{0.7}O_{3-\delta}$ and amorphous STO is present. It is enhanced by the doped Co ions at more than a 5 % content, however, as the Co content increases from 10 to 30 %, a new crystal phase, such as $SrCoO_3$, may appear and segregate to make the surface become unstable. The stability enhancement of the surface region by the presence of a small amount of Co ions and the suppression of the crystal stability caused by the extra amount of Co ions are responsible for the presence of the optimum Co content at 5-10 % in the thin films.

8. The absorption bands at 2-3 eV and at 3.4 eV in the Co-STO target are assigned as the d-d transition due to octahedral Co(II) ions and as charge-transfer bands due to Opπ to Co(II) transition, respectively.
9. The photo-catalytic activity under very weak visible light irradiation with a blue LED (460 nm, 0.7 mW) of the STO thin film is enhanced two times by the presence of Co. The quantum yields of Co-STO thinfilms correspond to the order of 1.67-5.76 x 10^{-4}.

REFERENCES

[1]C. Cen, S. Thiel, J. Mannhart, J. Levy, Science 323, 1026 (2009).

[2]A. Santander-Syro, O. Copie, T. Kondo, F. Fortuna, S. Pailhes, R. Weht, X. Qiu,F. Bertran, A. Nicolaou, A. Taleb-Ibrahimi, Nature 469, 189 (2011).

[3]M. S. Wrighton, A. B. Ellis, P. T. Wolczanski, D. L. Morse, H. B. Abrahamson, D. S. Ginley, J. Am. Chem. Soc. 98, 2774 (1976).

[4]M. S. Wrignton, P. T. Wolczanski, A. B. Ellis, J. Solid State Chem. 22, 17 (1977).

[5]K. Domen, A. Kudo, T. Onishi, N. Kosugi, H. Kuroda, J. Phys. Chem. 90, 292 (1986).

[6]H. Pan, Renew. Sustain. Energy Rev. 57, 584 (2016).

[7]H. Grabowska, Appl. Catal. B: Env. 186, 970 (2016).

[8]K. Shan, X-M. Guo, Mater. Lett. 113, 126 (2013).

[9]K. Shan, Z-Z. Yi, Scripta Mater. 107, 119 (2015).

[10]A. V. Kovalevsky, S. Populoh, S. G. Patrício, P. Thiel, M. C. Ferro, D. P. Fagg, J. R. Frade, A. Weidenkaff, J. Phys. Chem. C 119, 4466 (2015).

[11]D. Luo, W. Xiao, F. Lin, C. Luo, X. Li, Adv. Power Tech. 27, 481 (2016).

[12]S. Song, L. Xu, Z. He, J. Chen, X. Xiao, B. Yan, Environ. Sci. Technol. 41, 5846 (2007).

[13]S. Song, L. Xu, Z. He, H. Ying, J. Chen, X. Xiao, B. Yan, J. Hazard. Mater. 152, 1301 (2008).

[14]X. Yan, S. Sun, B. Hu, X. Wang, W. Lu, W. Shi, Micro & Nano Lett. 8, 504 (2013).

[15]R. Asahi, T. Morikawa, T. Ohwaki, K. Aoki, Y. Taga, Science 293, 269 (2001).

[16]H. Irie, Y. Watanabe, K. Hashimoto, J. Phys. Chem. B 107, 5483 (2003).

[17]S. Yoon, A. E. Maegli, L. Karvonen, S. K. Matam, A. Shkabko, S. Riegg, T. Groβman, S. G. Ebbinghaus, S. Pokrant, A. Weidenkaff, J. Solid State Chem. 206, 226 (2013).

[18]C. Zhang, Y. Jia, Y. Jing, Y. Yao, J. Ma, J. Sun, Comp. Mater. Chem. 79, 69 (2013).

[19]H. Kato, A. Kubo, J. Phys. Chem. B 106, 5029 (2002).

[20]T. Ohno, T. Tsubota, Y. Nakayama, K. Sayama, Appl. Catal. A. Gen 288, 74 (2005).

[21]M. Miyauchi, M. Takashio, H. Tobimatsu, Langmuir 20, 232 (2004).

[22]H. Irie, Y. Maruyama, K. Hashimoto, J. Phys. Chem. C 111, 1847 (2007).

[23]T. Ishii, H. Kato, A. Kudo, J. Photochem. Photobiol. A Chem. 163, 181 (2004).

[24]D. Wang, J. Ye, T. Kako, T. Kimura, J. Phys. Chem. B 110, 15824 (2006).

[25]J. W. Liu, G. Chen, Z. H. Li, Z. G. Zhang, J. Solid State Chem. 179, 3704 (2006).

[26]R. B. Comes, P. V. Sushko, S. M. Heald, R. J. Colby, M. E. Bowden, S. C. Chambers, Chem. Mater. 26, 7073 (2014).

[27]J. G. Bednorz, K. A. Müller, Phys. Rev. Lett. 52, 2289 (1984).

[28]S. K. Mishra, R. Ranjeev, D. Pandey, R. Ouillon, J. –P. Pinan-Lucarre, P. Ranson, Ph. Pruzan, Phys. Rev. B 64, 092302 (2001).

[29]V. V. lemanov, E. P. Smirnova, P. P. Syrnikov, E. A. Tarakanov, Phys. Rev. B54, 3151 (1996).

[30]V. V. lemanov, E. P. Smirnova, E. A. Tarakanov, Phys. Solid State 39, 628 (1997).

[31]C. Ang, Z. Yu, Phys. Rev. B 61, 11363 (2000).

[32]A. Tkach, P. M. Vilarinho, A. L. kholkin, Appl. Phys. Lett. 86, 172902 (2005).

[33]W. Chang, S. W. kirchoefer, J. M. Pond, J. S. Horwitz, J. Appl. Phys. 92, 1528 (2002).

[34]A. Tkach, T. M. Correia, A. G. Moreira, M. R. Chaves, O. Okhay, P. M. Vilarinho, I. Gregora, J. Petzelt, Acta Materialia 59, 5388 (2011).

[35]M. Ghaffari, T. Liu, H. Huang, O. K. Tan, M. Shannon, Mater. Chem. Phys. 136, 347 (2012).

[36]M. Ghaffari, M. Shannon, H. Hui, O. K. Tan, A. Irannejad, Surf. Sci. 606, 670 (2012).

[37]S. Fuentes, P. Muñoz, N. Barraza, E. Chávez-Ángel, C. M. S. Torres, J. Sol-Gel Technol. 75, 593 (2015).

[38]A. E. Bocquet, A. Fujimori, T. Mizokawa, T. Saitoh, H. Namatame, S. Suga, N. Kimizuka, Y. Takeda, M. Takano, Phys. Rev. B 45, 1561 (1992).

[39]S. Malo, A. Maignan, Inorg. Chem. 43, 8169 (2004).

[40]C. Pascanut, N. Dragoe, P. Berthet, J. Magn. Magn. Mater. 305, 6 (2006).

[41]C. Decorse-Pascanut, J. Berthon, L. Pinsard-Gaudart, N. Dragoe, P. Berthet, J. Magn. Magn. Mater. 321, 3526 (2009).

[42]D. Yao, X. Zhou, S. Ge, Appl. Surf. Sci. 257, 9233 (2011).

[43]S. Kawasaki, M. Takano, Y. Takeda, J. Solid State Chem. 121, 174 (1996).

[44]A. B. Posadas, C. Mitra, C. Lin, A. Dhamdhere, D. J. Smith, M. Tsoi, A. A. Demkov, Phys. Rev. B 87, 144422 (2013).

[45]H. T. Langhammer, R. Böttcher, T. Müller, T. Walther, S. Ebbinghaus, J. Phys.: Condens. Matter 27, 295901 (2015).

[46]S. Dugu, S. P. Pavunny, Y. Sharma, J. F. Scott, R. S. Katiyar, J. Appl. Phys. 118, 034105 (2015).

[47]K. G. Roberts, M. Varela, S. Rashkeev, S. T. Pantelides, S. J. Pennycook, K. M. Krishnan, Phys. Rev. B 78, 014409 (2008).

[48]C. Sena, M. S. Costa, E. L. Muñoz, G. A. Cabrera-Pasca, l. f. d. Pereira, J. Mestnik-Filho, A. W. Carbonari, J. A. H. Coaquira, J. Magn. Magn. Mater. 387, 165 (2015).

[49]S. X. Zhang, S. B. Ogale, D. C. Kundaliya, L. F. Fu, N. D. Browning, S. Dhar, W. Ramadan, J. S. Higgins, R. L. Greene, T. Venkatesan, Appl. Phys. Lett. 89, 012501 (2006).

[50]L. Bi, H-S. Kim, G. F. Dionne, C. A. Ross, New. J. Phys. 12, 043044 (2010).

[51]J. M. Florez, S. P. Ong, M. C. Onbaşli, G. F. Dionne, P. Vargas, G. Ceder, C. A. Ross, Appl. Phys. Lett. 100, 252904 (2012).

[52]C. Mitra, C. Lin, A. B. Posadas, A. A. Demkov, Phys. Rev. B 90, 125130 (2014).

[53]S. Gerhold, M. Riva, B. Yildiz, M. Schmid, U. Diebold, Surf. Sci. 651, 76 (2016).

[54]T. Ohsawa, K. Iwaya, R. Shimizu, T. Hashizume, T. Hitosugi, J. Appl. Phys. 108, 073710 (2010).

[55]R. Shimizu, T. Ohsawa, K. Iwaya, S. Shiraki, T. Hitosugi, Cryst. Growth Des. 14, 1555 (2014).

[56]K. Fuchigami, Z. Gai, T. Z. Ward, L. F. Yin, P. C. Snijders, E. W. Plummer, J. Shen, Phys. Rev. Lett. 102, 066104 (2009).

[57]A. Tselev, R. K. Vasudevan, A. G. Gianfrancesco, L. Qiao, P. Ganesh, T. L. Meyer, H. N. Lee, M. D. Biegalski, A. P. Baddorf, S. V. Kalinin, ACS Nano 9, 4316 (2015).

[58]A. Iwabuchi, C-K. Choo, K. Tanaka, J. Phys. Chem. B 108, 10863 (2004).

[59]K. Tanaka, K. Miyahara, I. Toyoshima, J. Phys. Chem. 88, 3504 (1984)

[60]D. Yao, X. Zhou, S. Ge, Appl. Surf. Sci. 257, 9233 (2011).

[61]P. Pertosa, F. M. Michel-Calendini, Phys. Rev. B 17, 2011 (1978).

[62]L. H. Hudson, R. L. Kurtz, S. W. Robey, D. Temple, R. L. Stockbauer, Phys. Rev. B 47, 1174 (1993).

[63]J. Kou, J. Gao, Z. Li, H. Yu, Y. Zhou, Z. Zou, Catal. Lett. 145, 640 (2015).

[64]C. Decorse-Pascanut, J. Arthon, L. Pinsard-Gaudart, N. Dragoe, P. Berthet, J. Magn. Magn. Mater. 321, 3526 (2009).

[65]A. Tkach, T. M. Correia, A. Almeida, J. Agostinho Moreira, M. R. Chaves, O. Okhay, P. M. Vilarinho, I. Gregora, J. Petzelt, Acta Mater. 59, 5388 (2011).

[66]I.Álvarez-Serrano, G. J. Cuello, M. L. López, A. Jiménez-Lópeg, C. Pino, E. Rodríguez-Castellón, E. Rodríguez, M. L. Veiga, J. Phys. D: Appl. Phys. 4, 1951001 (2008).

[67]R. Riva, H. Miessner, R. Vitali, G. Del Piero, Appl. Catal. A; Gen. 196, 111 (2000).

[68]A. A. Khassin, T. M. Yurieva, V. V. Kaichev, V. I. Bukhtiyarov, A. A. Budneva, E. A. Paukshtis, V. N. Parmon, J. Mol Catal. A 175, 189 (2001).

[69]N. V. Kosova, V. V. Kaichev, V. I. Bukhtiyarov, D. G. Kellerman, E. T. Devyatkina, T. V. Larina, J.Power Sources 119-121, 669 (2003).

[70]B. S. Jeong, Y. W. Heo, D. P. Norton, J. G. Kelly, R. Rairight, A. F. Hebard, J. D. Budai, Y. D. Park, Appl. Phys. Lett. 84, 2608 (2004).

[71]J. G. Li, R. Büchel, M. Isobe, T. Mori, T. Ishigaki, J. Phys. Chem. C 113, 8009 (2009).

[72]Y. Huang, B. Zhao, R. Ang, S. Lin, Z. Huang, S. Tan, Y. Liu, W. Song, Y. Sun, J. Phys. Chem. C 117, 11459 (2013).

[73]H. Oda, H. Yamamoto, H. Watanabe, J. Phys. Soc. Jpn. 44, 1391 (1978).

[74]B. J. Tan, K. J. Klabonde, P. M. A. Sherwood, J. Am. Chem. Soc. 113, 855 (1991).

[75]S. C. Petitto, E. M. Marsh, G. A. Carson, M. A. Langelli, J. Mol. Catal., A: Chem. 281, 49 (2008).

[76]C. Suchomski, C. Reitz, K. Brezesinski, C. T. Sousa, M. Rohnke, K. Iinuma, J. P. E. Araujo, T. Bregesinski, Chem Mater. 24, 155 (2012).

[77]A. G. Kochur, A. . Kozakov, K. A. Googlev, S. P. Kubrin, A. V. Nikolskii, V. I. Togashev, A. A. Bush, V. Ya. Shkuratov, S. I. Shevtsova, J.Alloy Comp. 636, 241 (2015).

[78]C. R. Brundle, T. J. Chuang, D. W. Rice, Surf. Sci. 60, 286 (1976).

[79]B. Gong, X. Luo, N. Bao, J. Ding, S. Li, J. Yi, Surf. Interface Anal. 46, 1043 (2014).

[80]H. Sekimoto, Y. Nose, T. Uda, H. Sugimura, Mater. Trans. 51, 2121 (2010).

[81]P. A. W. van der Heide, Surf. Interface Anal. 33, 414 (2002).

[82]D. Ehre, H. Cohen, V. Lyahovinskaya, I. Lubomirsky, Phys. Rev. B 77, 184106 (2008).

[83]J. –G. Kim, D. L. Pugmire, D. Battaglia, M. A. Langell, Appl. Surf. Sci. 165, 70 (2000).

[84]N. A. Marino, B. P. Barbero, P. Eloy, L. E. Cadús, Appl. Surf. Sci. 253, 1489 (2006).

[85]E. J. Crumlin, E. Mutoro, W. T. Hong, M. D. Biegalski, H. M. Christen, Z. Liu, H. Bluhm, Y. Shao-Horn, J. Phys. Chem. C 117, 16087 (2013).

[86]X. Cheng, E. Fabbri, M. Nachtegaal, I. E. Castelli, M. E. Kazzi, R. Haumont, N. Marzari, T. J. Schmidt, Chem. Mater. 27, 7662 (2015).

[87]T. E. Machonkin, M. D. Boshart, J. A. Schofield, M. M. Rodriguez, K. Grubel, D. Rokhasana, W. W. Brennessel, P. L. Holland, Inorg. Chem. 53, 9837 (2014).

[88]D. Schweinfurth, M. G. Sommer, M. Atanasov, S. Demeshko, S. Hohloch, F. Meyer, F. Neese, B. Sarkar, J. Am. Chem. Soc. 137, 1993 (2015).

[89]M. Idešicová , J. Titiš, J. Krzystek, R. Boča, Inorg. Chem. 52, 9409 (2013).

[90]J. M. Zadrozny, J. Telser, J. R. Rong, Polyhedron 64, 209 (2013).

[91]A. Eichhöfer, Y. Lan, V. Mereacre, T. Bodenstein, F. Weigend, Inorg. Chem. 53, 1962 (2014).

[92]Y. Yang, M. A. Ratner, G. C. Schats, J. Phys. Chem. C 118, 29196 (2014).

[93]K. Tanaka, C-K. Choo, R. Kobayashi, Japan Pat., No.5294207(2013.9.18)

[94]K. Tanaka, C-K. Choo, J. Ohta, Japan Pat., No. 5582522 (2014.9.3)

Figure Captions

FIG. 1. X-ray diffraction spectra of STO and Co-STO targets with Co contents of 1, 3, 5, 10, 20 and 30%.

FIG.2. Co 2p XPS spectra of Co(30)-STO target oxidized by O_2 at 1073K (a), after Ar sputtering (b: in situ), then exposed to air (c), reduced with H_2 at 1073 K (d) and re-oxidized with O_2 at 1073 K (e).

FIG. 3. Ti 2p XPS spectra of STO and Co(30)-STO targets. Treatments for notations a-e are the same as in Fig. 2.

FIG. 4. O 1s XPS spectra of STO and Co(30)-STO targets. Treatments for notations a-e are the same as in Fig. 2.

FIG. 5. The II/I intensity ratio for two kinds of O1s species, O(I) and O(II) at 530 and 533 eV, detected on STO and Co(30)-STO targets. Treatments are the same as in Fig. 2.

FIG. 6. Sr 3d XPS spectra of SrTiO and Co(30)-STO targets. Treatments for notations a-e are the same as in Fig. 2.

FIG. 7. Valence band spectra of STO and Co(30)-STO targets. Treatments for notations a-e are the same as in Fig. 2.

FIG. 8. Structure of STO

FIG. 9. Atomic ratio of Ti/Sr and Co/Sr on Co-STO targets, and PLA thin films prepared at r.t. and 873 K as a function of the Co content. Note that these values for the target and PLA thin films of the STO are shown as double marked symbols.

FIG. 10. The II/I intensity ratio for two kinds of O1s species, O(I) and O(II) at 530 and 533 eV, detected on the Co-STO targets, and PLA thin films prepared at r.t. and 873 K as a function of the Co content. Note that these values for the target and PLA thin films of STO are denoted as black symbols.

FIG 11. X-ray diffraction spectra of $SrTiO_3$(110) face for PLA thin films prepared at r.t. and 873 K using STO and Co(30)-STOtargets with Co contents of 1, 3, 5, 10, 20 and 30%.

FIG. 12. Tauc plots of r.t. and 873 K prepared STO thin films, Co(20)-STO target and the 873 K prepared thin film.

FIG. 13. The XRD intensities of PLA thin films prepared at r.t., then oxidized in O_2 at 873 and 973 K, or reduced with H_2 at 873, 973 and 1073 K. Targets used for PLA were STO and Co-STO targets with Co contents of 3, 10 and 30%.

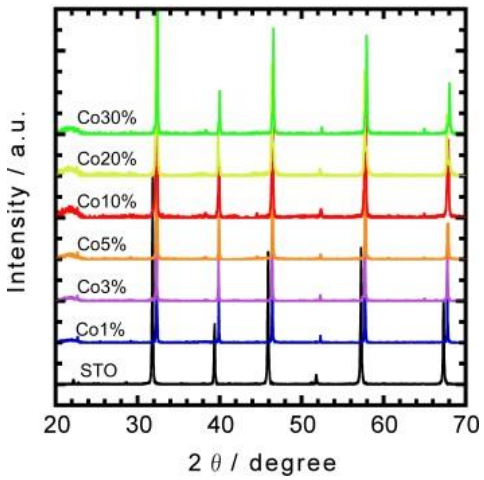

FIG. 1.

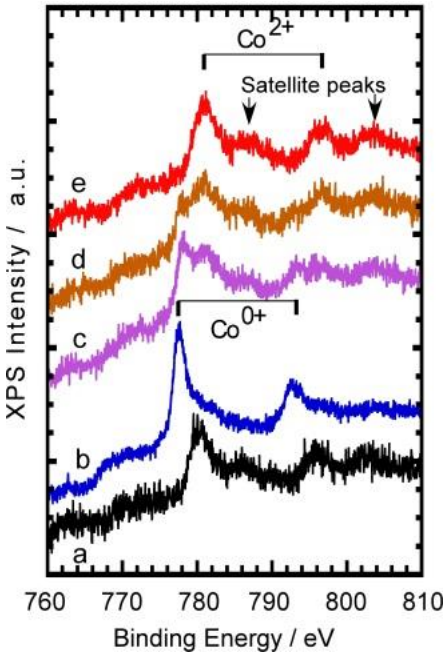

FIG. 2

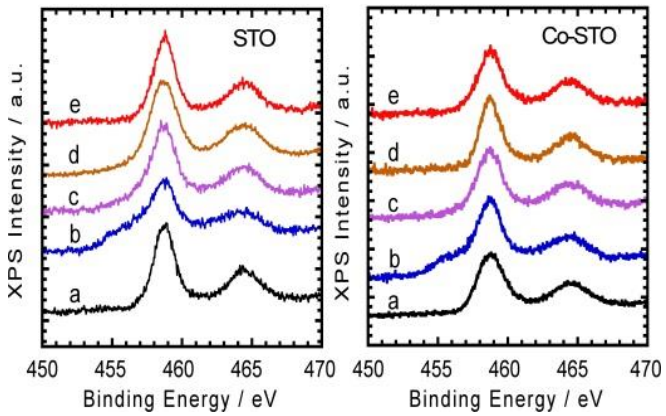

FIG. 3

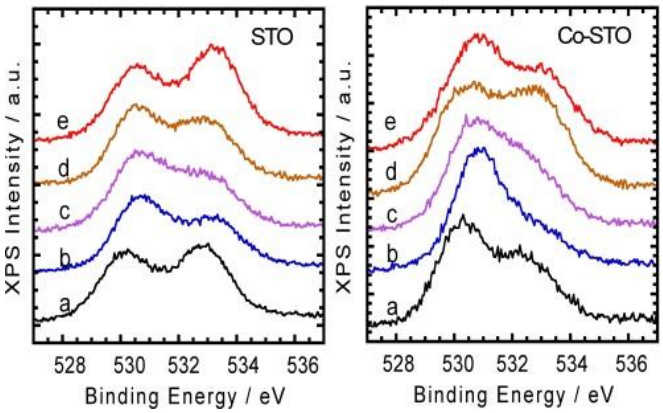

FIG. 4

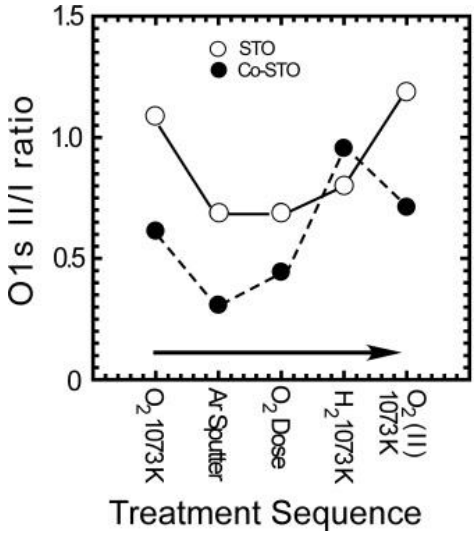

FIG. 5

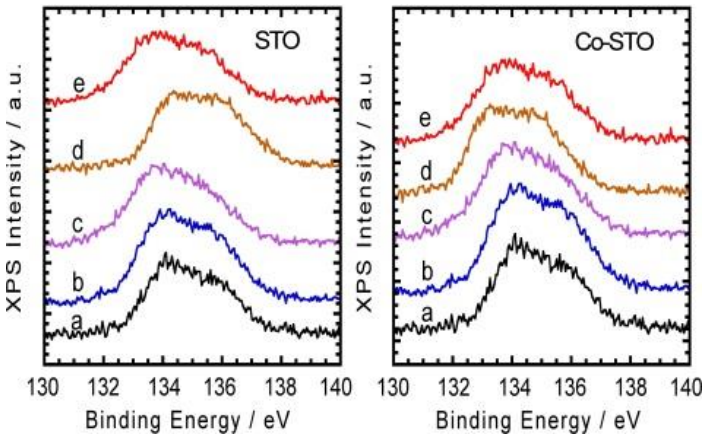

FIG. 6

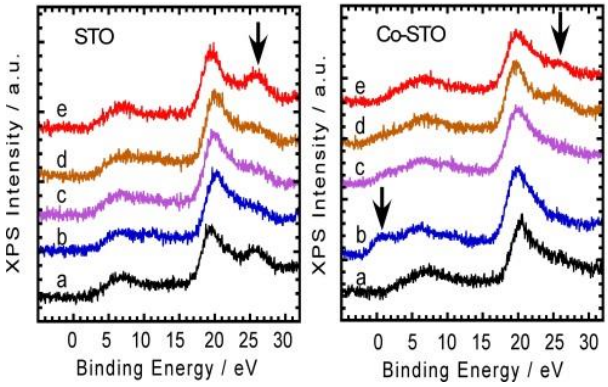

FIG. 7

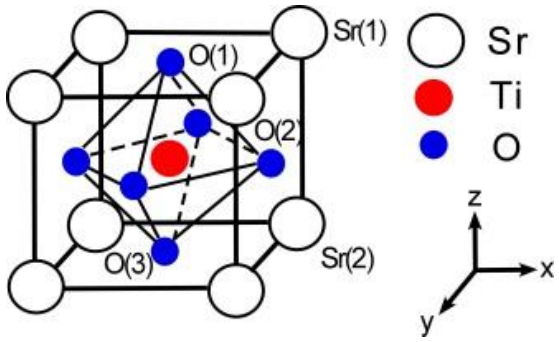

FIG. 8

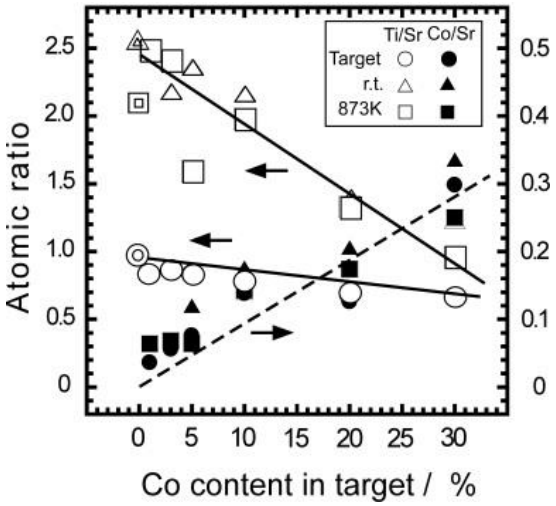

FIG. 9.

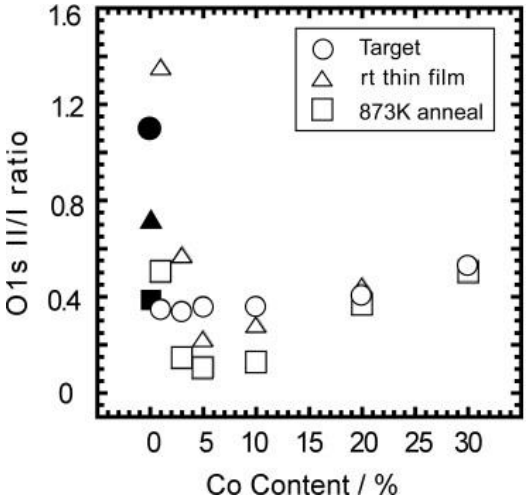

FIG. 10

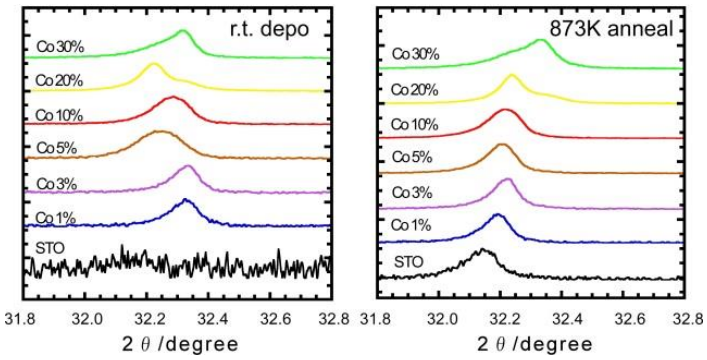

FIG 11

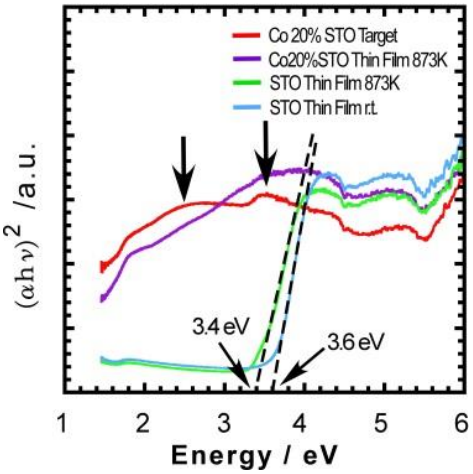

FIG. 12

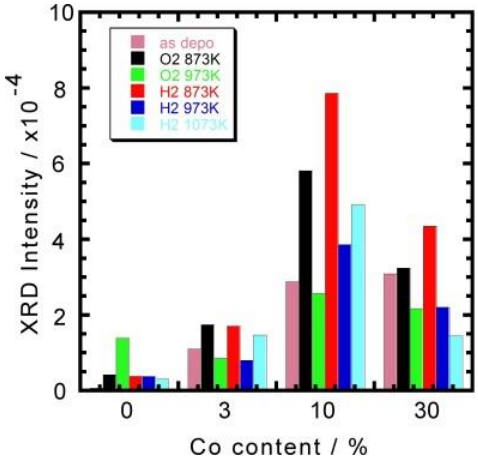

FIG. 13